Available online at www.sciencedirect.com

ScienceDirect

journal homepage: www.elsevier.com/locate/he

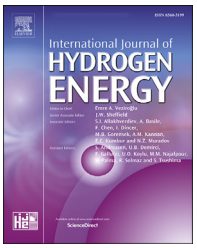

Grand Canonical Monte Carlo simulations of the hydrogen storage capacities of slit-shaped pores, nanotubes and torusenes

D. Caviedes, I. Cabria *

Departamento de Física Teórica, Atómica y Óptica, Universidad de Valladolid, 47011, Valladolid, Spain

HIGHLIGHTS

- Hydrogen Storage Capacities of Torusenes.
- Hydrogen Storage Capacities of Three Types of Pores.
- Quantitative Structure-Hydrogen Storage Capacities of Porous Materials.

ARTICLE INFO

Article history:
Received 23 September 2021
Received in revised form
28 January 2022
Accepted 29 January 2022
Available online xxx

Keywords:
Hydrogen storage
Hydrogen physisorption
Nanoporous carbons
Grand canonical Monte Carlo simulations

ABSTRACT

Grand Canonical Monte Carlo, GCMC, simulations are used to study the gravimetric and volumetric hydrogen storage capacities of different carbon nanopores shapes: Slit-shaped, nanotubes and torusenes at room temperature, 298.15 K, and at pressures between 0.1 and 35 MPa, and for pore diameter or width between 4 and 15 Å. The influence of the pore shape or curvature on the storage capacities as a function of pressure, temperature and pore diameter is investigated and analyzed. A large curvature of the pores means, in general, an increase of the storage capacities of the pores. While torusenes and nanotubes have surfaces with more curvature than the slit-shaped planar pores, their capacities are lower than those of the slit-shaped pores, according to the present GCMC simulations. Torusene, a less studied carbon nanostructure, has two radii or curvatures, but their storage capacities are similar or lower than those of nanotubes, which have only one radius or curvature. The goal is to obtain qualitative and quantitative relationships between the structure of porous materials and the hydrogen storage capacities, in particular or especially the relationship between shape and width of the pores and the hydrogen storage capacities of carbon-based porous materials.

Introduction

Hydrogen vehicles are clean and environmentally friendly and therefore, they are an alternative to the fossil fuel-based vehicles. The use of these type of vehicles is a mean to fight against global warming and climate change. These vehicles have not yet been deployed in a large scale, because there is not a cheap and efficient method to store enough hydrogen

* *Corresponding author.*
E-mail address: ivan.cabria@uva.es (I. Cabria).

https://doi.org/10.1016/j.ijhydene.2022.01.229

on-board. There are two on-board hydrogen storage standards. The Department of Energy, DOE, on-board hydrogen storage targets for 2020 are 0.030 kg H_2/L and 4.5 wt % for the volumetric and gravimetric storage capacities, respectively, and for 2025 are 0.040 kg/L and 5.5 wt % [1,2]. The ultimate storage targets are 0.050 kg H_2/L and 6.5 % wt. These values or targets would allow us to store enough hydrogen to have the same autonomy range as the fossil fuel based vehicles, about 600 km.

The Toyota Mirai 2018 vehicle can be considered a second standard. This is a commercial vehicle whose tanks store compressed hydrogen at 70 MPa in a total volume of 122.4 L. It has a gravimetric capacity, g_c, of 5.7 wt %, a volumetric capacity, v_c, of 0.040 kg/L and an autonomy of 312 miles (502 km) [3,4].

There are three types of on-board hydrogen storage: liquid, compressed gas, and solid, which comprises chemical storage and storage by physical adsorption. Solid storage by physical adsorption consists on storing hydrogen gas by physisorption in the pores of solid porous materials. According to experiments the storage by physisorption on porous materials is fully reversible at low and room temperatures [5,6]. This storage type allows us to store more hydrogen at lower pressures ($\leq$25 MPa) than the compressed gas storage type (70 MPa). The goal is to obtain solid porous materials that meet or exceed the DOE targets or the benchmarks of Toyota Mirai, using tanks that operate at moderate pressures, which are less expensive. There is an intense research to find that kind of solid porous materials for hydrogen storage [7–10]. The most promising groups of solid porous materials for hydrogen storage are nanoporous carbons [3,11,12], porous aromatic frameworks (PAFs) [13], covalent organic frameworks (COFs) [14,15], porous polymer networks (PPNs) [16–18], metal-organic frameworks (MOFs) [19,20], and polymers of intrinsic microporosity (PIMs) [21,22], due to their large free pore volume and specific surface area.

Nanoporous carbons are a family or type of solid porous materials that has received much attention as a potential material for hydrogen storage [3,11,12]. The structure of nanoporous carbons is a network of nanopores of different shapes and sizes. According to experimental reports, many regions of these carbon-based materials are flat graphitic-like surfaces parallel to each other and separated a few nanometers [23–25]. These regions receive the name of slit or slit-shaped pores. This is also the simplest and most used geometric shape of carbon nanopores in theoretical studies.

One of the properties of nanoporous carbons that has an important impact on their hydrogen storage capacities is the shape or the curvature of the pores. A curved surface interacts more strongly with a H_2 molecule than a flat surface and this could increase the amount of H_2 stored on pores with curved surfaces or shapes [26,27]. However, nanostructures with curved surfaces, like nanotubes and torusenes, usually have a larger surface mass density of the adsorbent material than planar surfaces, like slit-shaped pores, and this decreases the gravimetric capacity. Hence, the net gravimetric capacity depends on a balance between mass of the adsorbent material and stronger interaction energies with the hydrogen molecules.

Torusenes are a little explored type of carbon nanostructure, in contrast with slit-shaped carbon pores and nanotubes, which have been intensively studied and analyzed, not only for gas storage purposes. Torusenes have been synthesized by several experimental groups [28–36] and some of their properties have been studied theoretically [37–44]. Synthesized torusenes have radii greater than 150 nm. A torusene consists on an sp2-hybridized pure carbon structure in the shape of a torus or doughnut. These structures received different names in the literature: torusenes, nanotori, toroidal polyhexes, carbon nanorings (CNRs), carbon nanotube rings, carbon nanorings and nanotube tori. The toroidal structure of the torusenes has two radii or curvatures, while nanotubes have only one radius or curvature and slit-shaped pores have no curvature.

There are many first principles calculations and GCMC simulations of the physisorption and storage of hydrogen on different nanoporous structures [45–56]. Karki and Chakraborty [45], Kumar et al. [52], García Blanco et al. [53] and Cracknell [54] performed GCMC simulations of the hydrogen storage on slit-shaped pores. GCMC simulations of the hydrogen storage capacities of both, slit-shaped and nanotubes, were carried out by Wang and Johnson [55] and Rzepka et al. [56]. However, to the extent of our knowledge, the hydrogen storage capacities of torusenes have not been studied and there is a lack of comparison of the hydrogen storage capacities for three carbon pore shapes: planar, cylindrical and toroidal, to find and assess the relationship between the pore shape and width and the hydrogen storage capacities of carbon-based porous materials. The goals of the present research is to study the hydrogen storage capacities of torusenes and to find that relationship. Grand Canonical Monte Carlo, GCMC, simulations [57] of the hydrogen storage capacities of the three shapes of carbon pores: Slit-shaped, nanotubes and torusenes, have been carried out and analyzed. The simulations have been performed using an in-house code. This paper is organized as follows: Section: Methodology is devoted to the details of the Methodology used, the GCMC simulations, and the description of the pores studied. The hydrogen storage capacities of torusenes are presented and discussed in Section: Comparison of the hydrogen storage capacities of slit-shaped pores, nanotubes and torusenes. The comparison of the storage capacities of the three types of pores is the purpose of Section: Conclusions and future lines.

Methodology

GCMC simulations

The GCMC simulations of the gravimetric and volumetric hydrogen storage capacities of three carbon pore shapes (nanotube, slit-shaped pore and torusene) have been carried out at 298.15 K and for the pressures 0.1, 0.5 and the interval 1–25 MPa. A few simulations have been carried out at 30 and 35 MPa. The diameter of the slit-shaped, cylindrical and toroidal pores was in the range 4 and 15 Å. A wide pore of about 25 Å width was also studied for the three mentioned types of pore shapes plus for a spherical pore of the same

Please cite this article as: Caviedes D, Cabria I, Grand Canonical Monte Carlo simulations of the hydrogen storage capacities of slit-shaped pores, nanotubes and torusenes, International Journal of Hydrogen Energy, https://doi.org/10.1016/j.ijhydene.2022.01.229

width. In a GCMC simulation the system (adsorbent plus hydrogen molecules) is simulated in the Grand Canonical ensemble, which means that the volume, the chemical potential and the temperature of the system are constant along all the iterations of the simulation.

The Lennard-Jones, LJ, potential [58] has been used to simulate the H_2–H_2 in all the systems studied. The LJ potential has been used to simulate the C–H_2 interactions in the torusenes. The LJ parameters for the H_2–H_2 and C–H_2 interactions were obtained from Rzepka et al. [56] (See Table 1).

In the present GCMC simulations, the Steele potential [59] was used for the graphene-H_2 interaction in the slit pores, the Tjatjopoulos potential [60] for the nanotube-H_2 interaction in the cylindrical pores or nanotubes and the Siderius-Gelb potential [61] for the sphere-H_2 interaction in the spherical pores. The Steele, Tjatjopoulos and Siderius-Gelb potentials use the LJ parameters of the C–H_2 interaction. The chemical potential used in the GCMC simulations was the one derived from the Soave-Redlich-Kwong, SRK, equation of state [62], using for the acentric factor, the critical pressure and the critical temperature, the values published by Zhou and Zhou [63]: 0.216, 1.28 MPa and 33.2 K, respectively. There are more refined approaches to obtain the chemical potential. Moore and Wheeler [64] calculated the chemical potential of LJ fluid for different values of the density, using the Widom method, the CPP (Chemical Potential Perturbation) method and using directly the equation of state of the LJ fluid. The differences between the obtained chemical potentials were very small, but the computation time of the Widom and CPP methods was high.

The number of iterations was 10 million in each GCMC simulation. The number of iterations to reach the equilibrium was set to 5 million. The next 5 million iterations were used to calculate the capacities. The Metropolis algorithm was used in each iteration [65]. The 20% of the trials or attempts of the Metropolis algorithm consisted on the movement of one molecule, the 40% on the removal of one molecule and the remaining 40% consisted on the addition of one molecule. Several tests were performed to obtain these percentages.

The SRK equation of state and the LJ potentials were also tested. GCMC simulations of pure H_2 molecules in a simulation box of $50 \times 50 \times 50$ Å^3 at 298.15 K and at several values of the 'experimental' or input pressure were carried out. In each simulation or run the pair distribution function $g(r)$ is calculated from the positions of the molecules obtained in 50 000 configurations of that simulation. The pair distribution function is used to compute the calculated pressure, P_{calc}, by means of [66,67]:

$$P_{calc} = \frac{Nk_BT}{V} - \frac{2\pi N^2}{3V^2}\int_0^\infty r^3 U(r) g(r) dr, \quad (1)$$

where N is the average number of H_2 molecules in the simulation box, k_B is the Boltzmann constant, T is the temperature and V the volume of the simulation box and $U(r)$ is the LJ interaction potential between the molecules.

The results of the comparison of the pressures are plotted in Fig. 1 in the range of pressures studied in this work. The agreement between the calculated and input pressures is good. Another test consisted on the comparison of the density of hydrogen obtained directly from the SRK EOS and the density obtained in the GCMC simulations of pure hydrogen at 298.15 K and pressures between 0.1 and 25 MPa. That comparison is plotted in Fig. 2. There is also a good agreement between these two densities.

Description of the simulation cells of the pores

The geometries of the slit-shaped pore, the nanotube and the spherical pore have been plotted in Fig. 3.

The dimensions of the simulation cells of the systems studied have been chosen to obtain a volume that is not too large, to avoid too much computational load, and that can contain enough H_2 molecules inside (about 200–2000 molecules) for the range of pressure studied and the room temperature. The exact number of molecules, and hence, the volume of the simulation cell, depends on the pressure, the type of pore and the geometric parameters of the pore.

The simulation box of the slit-shaped pore consists on two graphene layers separated a distance w. The graphene layers lie in the xy plane. Periodic boundary conditions are applied to the simulation box of slit pores in the x and y directions. Each layer has lengths of 88.54 and 89.46 Å along the x and y axes, respectively. These lengths of the graphene layers are consistent with the periodic boundary conditions of graphene. The simulated slit pores have a distance or width w between 4 and 15 Å. A slit pore with $w = 25.089$ Å has been also analyzed. The volume of the simulation cell of a slit-shaped pore is SD, where S is the surface area, $S = 88.54 \times 89.46$ Å^2, and D is the width of the pore. The volumes of the simulated slit-shaped pores are between 32 000 and 120 000 Å^3, plus one simulation cell of 199 000 Å^3, that corresponds to $w = 25.089$ Å.

Table 1 – LJ parameters used in the GCMC simulations. σ is in Å and ε in eV. The values were taken from Rzepka et al. [56].

Atoms or molecules	σ	ε
C–H_2	3.190	0.002 628
H_2–H_2	2.970	0.002 870

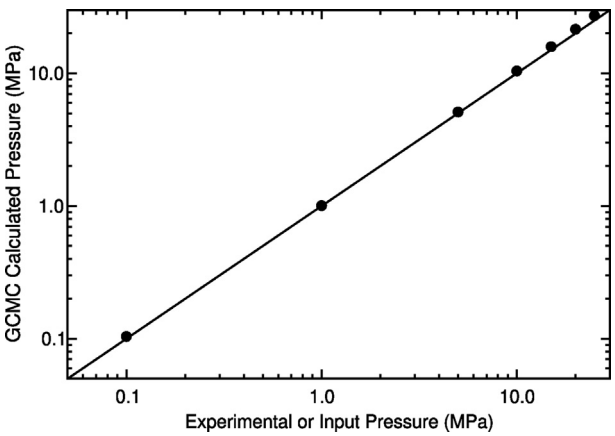

Fig. 1 – GCMC calculated pressure vs the 'experimental' or input pressure, obtained in the simulations of pure H_2 at 298.15 K.

Please cite this article as: Caviedes D, Cabria I, Grand Canonical Monte Carlo simulations of the hydrogen storage capacities of slit-shaped pores, nanotubes and torusenes, International Journal of Hydrogen Energy, https://doi.org/10.1016/j.ijhydene.2022.01.229

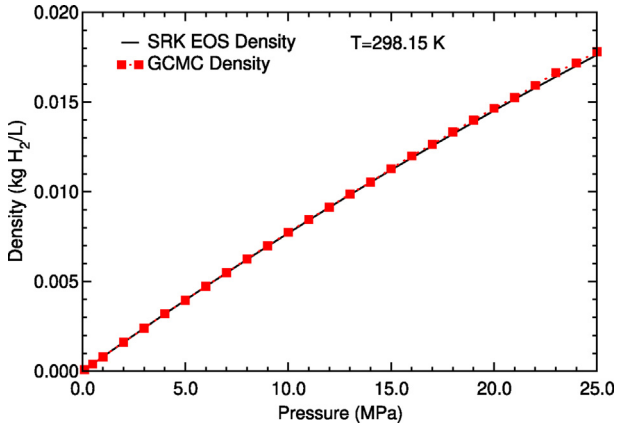

Fig. 2 – SRK EOS density and GCMC density obtained in the simulations of pure H_2 vs pressure, at 298.15 K.

Nanotubes with a diameter between 4 and 15 Å and one nanotube with a wide diameter of 25.089 Å have been simulated. The nanotube (19,18) has a diameter of 25.089 Å and is the nanotube with the closest diameter to 25 Å. In the case of nanotubes, the periodic boundary conditions are applied in the direction of the main axis of the nanotube. The length L of the nanotube of the simulation cell is consistent with the periodic conditions. The simulation box of the nanotubes has a length L such that the volume of the nanotube is approximately 88 000 Å^3 or the closest value. The volume of the nanotube of the simulation cell is $\pi r^2 L$, where r is the radius of the nanotube. The volumes of the nanotubes with a diameter between 4 and 15 Å are between 77 000 and 88 000 Å^3 and their tube lengths L are between 6770 and 470 Å. The widest nanotube simulated, (19,18), has a length of 136.5 Å and a volume of about 67 500 Å^3. The value of 88 000 Å^3 for the volume of nanotubes has been selected after some tests, to have enough H_2 molecules inside the nanotube, as it was explained above.

Torusenes are closed structures and hence, periodic boundary conditions are not applied to their simulation boxes, which contain their geometric structures. Torusenes have two radius. Torusenes with an external radius R of 20, 70 and 240 Å, and an internal radius r between 2.4 and 7.5 Å, have been simulated. Torusenes with an internal diameter of 25.089 Å have been also simulated. The volume of the simulation cell of a torusene is $2\pi^2 r^2 R$, where r is the internal radius. Hence, the simulation cells of the torusenes with an external radius of 20 Å have volumes between 1600 and 22 000 Å^3, those of torusenes with $R = 70$ Å have volumes between 5500 and 78 000 Å^3 and the simulation cells of the torusenes with $R = 240$ Å have volumes between 19 000 and 266 000 Å^3. The torusenes with a diameter of 25.089 Å and R = 20, 70 and 240 Å have volumes of 62 000, 217 000 and 746 000 Å^3, respectively. A description of the geometry and coordinates of the carbon atoms of the torusenes is explained in a section below.

As regards to spherical pores, due to their spherical shape, their storage capacities are very small and only a wide spherical pore, with a diameter of 25.089 Å, have been simulated, to compare the results with the results obtained for slit-shaped pores, nanotubes and torusenes of the same width or diameter. The volumes of the simulation cells of the pores studied are summarized in Table 2.

Description of the torusenes

A torus or toroid is a surface generated by a circumference that rotates around an external straight line. This line does not intersect with circumference. A doughnut and a tyre chamber are daily objects with the shape of a torus. The Cartesian coordinates of a point on the surface of a torus are given by:

$$\begin{aligned} x &= \cos\beta(R + r\cos\alpha) \\ y &= \sin\beta(R + r\cos\alpha) \\ z &= r\sin\alpha. \end{aligned} \quad (2)$$

Table 2 – Volumes of the simulation cells (in Å^3) and range of diameters D (in AA) of the pores studied in the GCMC simulations.

Pore	D	Volume equation	Volume
Slit	4–15	SD	32 000–120 000
Nanotubes	4–15	$\pi r^2 L$	77 000–88 000
Torusenes R = 20	4.8–15	$2\pi^2 r^2 R$	1600-22 000
Torusenes R = 70	4.8–15	$2\pi^2 r^2 R$	5500-78 000
Torusenes R = 240	4.8–15	$2\pi^2 r^2 R$	19 000–266 000
Slit	25.089	SD	199 000
Nanotubes	25.089	$\pi r^2 L$	67 000
Torusenes R = 70	25.089	$2\pi^2 r^2 R$	217 000
Spherical Pore	25.089	$4\pi r^3/3$	8300

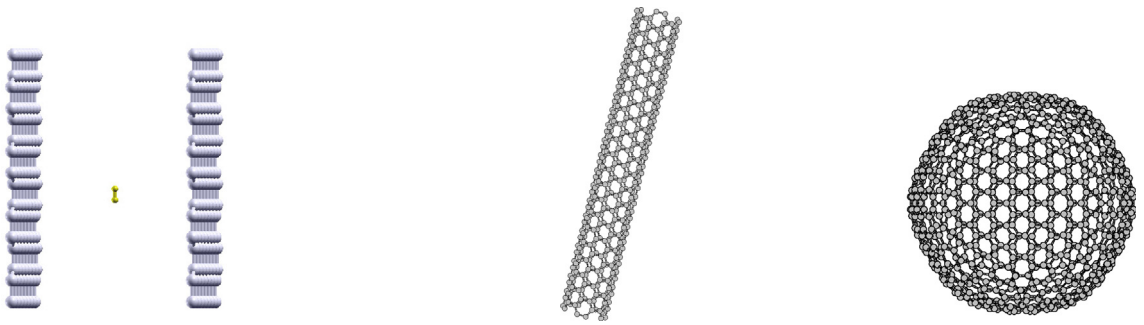

Fig. 3 – From left to right: Graphene slit-shaped pore with one H_2 molecule inside, (5,5) carbon nanotube (a diameter of 6.78 Å) and a spherical pore (a diameter of 25.089 Å).

Please cite this article as: Caviedes D, Cabria I, Grand Canonical Monte Carlo simulations of the hydrogen storage capacities of slit-shaped pores, nanotubes and torusenes, International Journal of Hydrogen Energy, https://doi.org/10.1016/j.ijhydene.2022.01.229

The magnitudes r and R are the internal radius and the external radius, respectively. By changing the values of the angles α and β, different points on the surface of the torus can be obtained.

The nanostructure composed by carbon atoms on the surface of a torus is called torusene (See Fig. 4). The procedure to generate the coordinates of the carbon atoms of the torusenes is described in the Appendix.

Hydrogen storage capacities of torusenes

Torusenes have two radii: The internal radius r and the external radius R. GCMC simulations of the hydrogen storage on torusenes with R = 20, 70 and 240 Å, and with internal radius r in the range 2.4–7.5 Å (internal diameter between 4.8 and 15 Å) and with a wide internal diameter of 25.089 Å, have been carried out at room temperature and for pressures in the range 0.1–35 MPa. The storage capacities obtained in the simulations of these torusenes are plotted in Figs. 5–7. These capacities will be analyzed as a function of the internal radius and of the pressure.

The storage capacities as a function of the internal diameter d, at 298.15 K and 25 MPa, are plotted in Fig. 5. Both, the gravimetric and volumetric capacities of torusenes with R = 20, 70 and 240 Å are very similar (the differences are very small), for the same value of the internal radius. The external radii of the three torusenes studied are very different.

The gravimetric capacity of the torusenes has a local maximum at $d = 6.8$ Å (See Fig. 5), and the volumetric capacity has the global maximum also at $d = 6.8$ Å.

The dependence of the storage capacities on the pressure can be noticed on Figs. 6 and 7. The storage capacities of torusenes with R = 20, 70 and 240 Å are, again, very similar, for fixed values of the other variables of the system: The internal radius ($r = 3.39$ and 12.544 Å), the temperature and the pressure. The internal radii r studied in these plots are very different, but in both Figures, the capacities do not depend on R.

According to the capacities obtained in the simulations and plotted in Figs. 5–7 for different pressures, and internal radii, the capacities of torusenes do not depend on their external radius R. It seems that the relevant part of the torusenes geometry for the storage capacities, is the internal radius r.

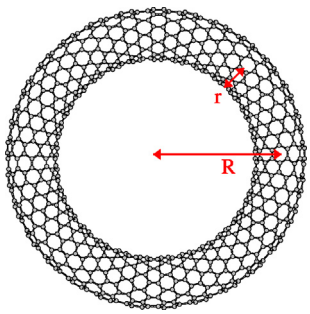

Fig. 4 – Top view of a carbon torusene with an external radius R of 20 Å and an internal radius r of 4 Å.

It is possible to get more insight into the independence of the results on the external radius R by plotting and analyzing the potential energy inside the torusenes, as a function of the molecule position with respect to the center of the torusene. The interaction potential energies inside six torusenes (R = 20, 70 and 240 Å; $r = 3.39$ and 12.544 Å) are plotted in Fig. 8. It can be noticed that the interaction potential energy practically does not depend on the external radius R. For the same internal radius r, the interaction potential energy of the three torusenes (R = 20, 70 and 240 Å) is very similar, is practically the same. This explains that the storage capacities obtained in the simulations do not depend on R.

Comparison of the hydrogen storage capacities of slit-shaped pores, nanotubes and torusenes

Hydrogen storage capacities of narrow slit-shaped pores, nanotubes and torusenes as a function of the pore width

The storage capacities obtained in the GCMC simulations of narrow slit-shaped graphene pores, carbon nanotubes and carbon torusenes are plotted and compared in Fig. 9. In those figures, pore width means the distance between the two graphene layers, in the case of slit-shaped pores, the tube diameter, in the case of nanotubes, and the torusene internal diameter, $2r$, in the case of torusenes. These are narrow pores: The pore width is between 4 and 15 Å.

The results obtained for slit-shaped pores are similar to the GCMC results published previously by several research groups. At 10 MPa and 298.15 K the total gravimetric storage capacity for a slit-shaped pore width of 12 Å obtained in the present simulations is 1.43 wt %. Wang and Johnson [55] and Cracknell [54] obtained at 10 MPa and 298 K a value of approximately 1.5 wt %, and Kumar et al. [52] a value of 1.47 wt % at 9.7 MPa and 298 K, for a pore width of 12 Å. The volumetric and gravimetric capacities of a slit-shaped pore of width 6.78 Å at 30 MPa and 298.15 K are 0.0216 kg/L and 0.95 wt %, respectively. Rzepka et al. [56] obtained volumetric and gravimetric capacities of 0.0235 kg/L and 0.95 wt %, respectively, at 30 MPa and 300 K for a pore width of 7 Å.

The gravimetric and volumetric capacities of nanotubes and torusenes, with the same pore width, are very similar; the differences are very small (See both panels of Fig. 9). It can also be noticed in that Figure that the gravimetric hydrogen storage capacities of slit-shaped pores are larger than the gravimetric capacities of nanotubes and torusenes. They are about two times larger for pores with a width equal or larger than 6.4 Å. As regards to the volumetric hydrogen storage capacities, the slit-shaped pores have larger volumetric capacities than the nanotubes and torusenes in some intervals of pore widths: Below 6.4 Å and between 7.8 and 10 Å. The maximum relative difference between the volumetric capacities of slit-shaped pores and nanotubes and torusenes in the interval 6.4–10 Å is about 12%. Beyond a pore width of 10 Å, the differences between the volumetric capacities of slit-shaped pores and nanotubes and torusenes are very small.

The volumetric capacities of the three types of pores seem to tend towards a common value as the pore width increases; they tend towards 0.018 kg of H_2/L. GCMC simulations carried out at

Please cite this article as: Caviedes D, Cabria I, Grand Canonical Monte Carlo simulations of the hydrogen storage capacities of slit-shaped pores, nanotubes and torusenes, International Journal of Hydrogen Energy, https://doi.org/10.1016/j.ijhydene.2022.01.229

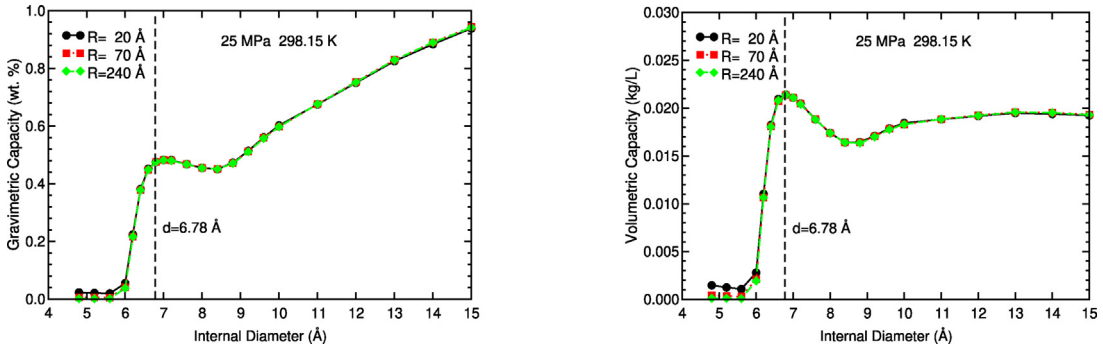

Fig. 5 – Total gravimetric and volumetric storage capacities of torusenes as a function of the internal diameter at 298.15 K and 25 MPa, and for external radii $R = 70$ and $R = 240$ Å.

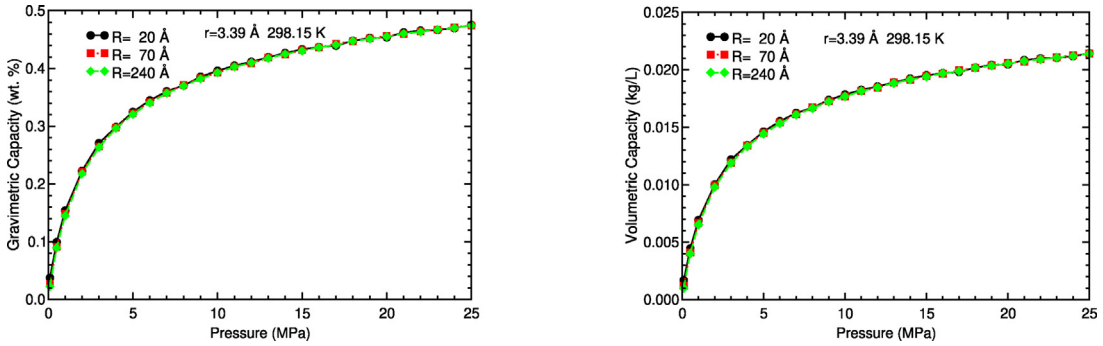

Fig. 6 – Total gravimetric and volumetric storage capacities of torusenes as a function of the pressure, at 298.15 K, for external radii $R = 20$, 70 and 240 Å, and an internal radius of 3.39 Å.

25 MPa and 298.15 K of a bulk free H_2 gas, in the same conditions as the present simulations, yielded a density of 0.017814 kg of H_2/L. Hence, the volumetric capacities of the three types of pores tend towards the bulk free hydrogen gas density. Previous GCMC simulations of slit-shaped pores and nanotubes also showed that the storage capacities of slit-shaped pores are larger than those of nanotubes of the same pore width [52,55,56] and that the volumetric capacities tend towards the bulk free hydrogen gas density as the pore width increases [56].

These results indicate that the higher curvature of torusenes and nanotubes, with respect to the planar surfaces of the slit-shaped pores, does not imply, in general, larger storage capacities. The slit-shaped pores have larger gravimetric capacities and their volumetric capacities are larger than those of nanotubes and torusenes for certain intervals of pore widths.

The gravimetric capacities of the three types of pores have the local maximum at the same pore width, 6.8–7 Å. The volumetric capacities of the three types of pores have the global maximum at the same pore width or diameter, $D = 6.8$ Å. Hence, the optimal pore size seems to be independent of the shape of the pores.

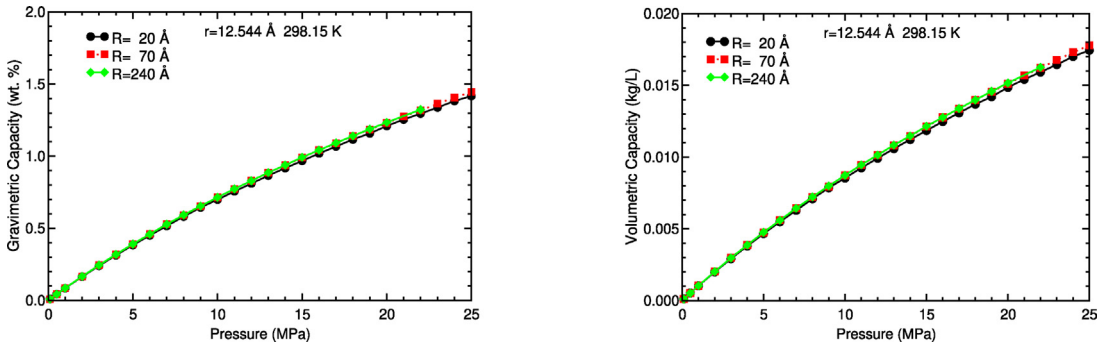

Fig. 7 – Total gravimetric and volumetric storage capacities of torusenes as a function of the pressure, at 298.15 K, for external radii $R = 20$, 70 and 240 Å, and an internal radius of 12.544 Å.

Please cite this article as: Caviedes D, Cabria I, Grand Canonical Monte Carlo simulations of the hydrogen storage capacities of slit-shaped pores, nanotubes and torusenes, International Journal of Hydrogen Energy, https://doi.org/10.1016/j.ijhydene.2022.01.229

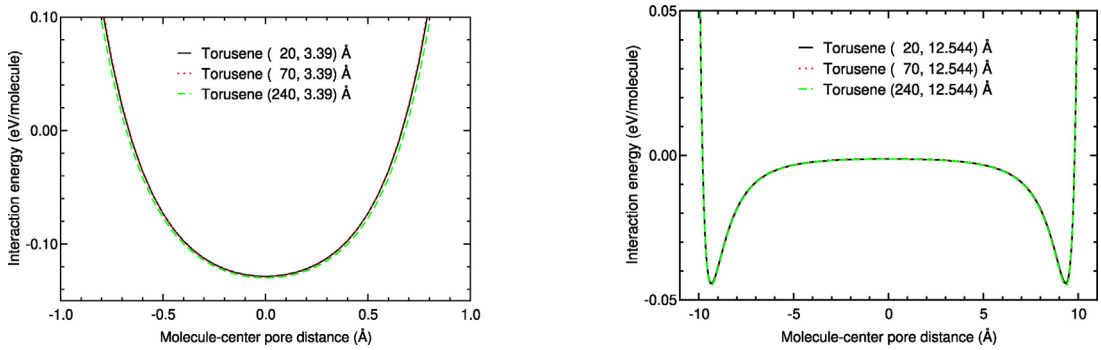

Fig. 8 – Interaction potential energy inside torusenes with external radii $R = 20$, 70 and 240 Å and with internal radii $r = 3.39$ and 12.544 Å.

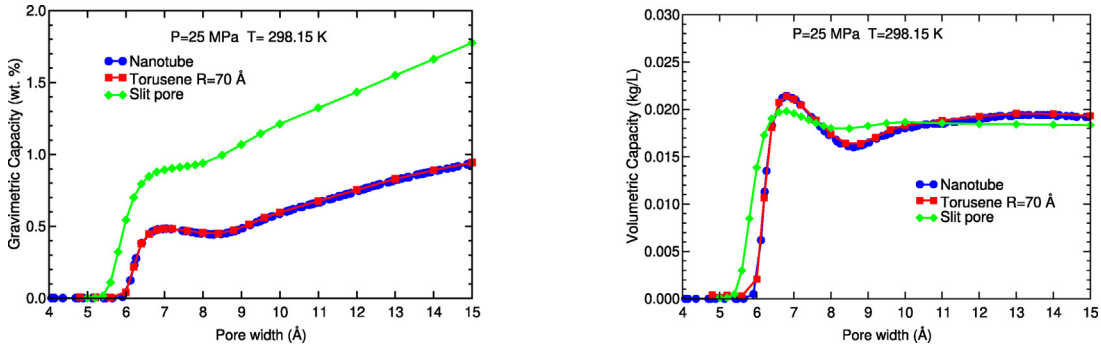

Fig. 9 – Total gravimetric and volumetric storage capacities of three pore shapes as a function of the pore width, at 25 MPa and 298.15 K.

Hydrogen storage capacities of narrow slit-shaped pores, nanotubes and torusenes of the same width as a function of the pressure

The hydrogen storage capacities of the three pore shapes, with the same narrow diameter, 6.78 Å, as a function of pressure and at 298.15 K, the so-called isotherms, obtained in the GCMC simulations are plotted in Fig. 10. The narrow diameter of 6.78 Å correspond to the local and maximum of the storage capacities of the three pores as a function of the pore size. The pressure was varied between 0.1 and 35 MPa.

The gravimetric and volumetric storage isotherms of the nanotube and torusene increase fast with the pressure and then, they tend towards a constant. The gravimetric and volumetric storage isotherm of the slit-shaped pore, however, increases slowly with the pressure and almost following a straight line.

The volumetric storage capacities of the nanotube and torusene are larger than those of the slit-shaped pore up to 32 MPa. Above that pressure, the volumetric capacities of the slit-shaped pore overcome those of the nanotube and torusene (See Fig. 10). As regards to the gravimetric storage

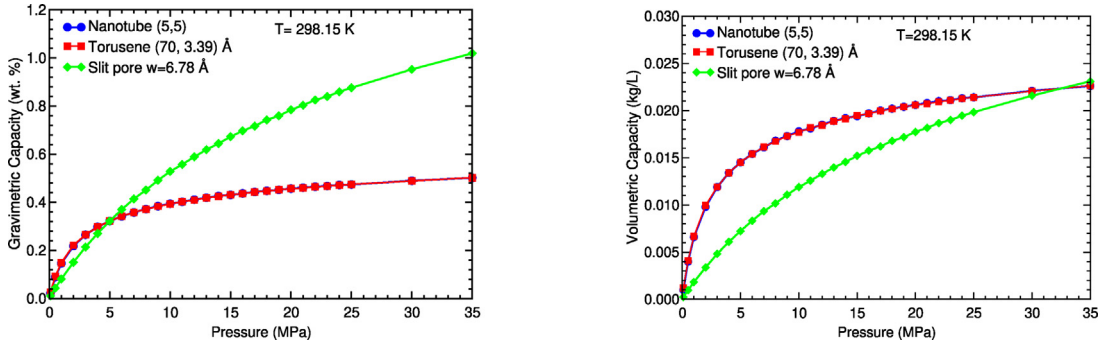

Fig. 10 – Total gravimetric and volumetric storage capacities of three pore shapes as a function of the pressure, at 298.15 K, and for a width or diameter of 6.78 Å.

Please cite this article as: Caviedes D, Cabria I, Grand Canonical Monte Carlo simulations of the hydrogen storage capacities of slit-shaped pores, nanotubes and torusenes, International Journal of Hydrogen Energy, https://doi.org/10.1016/j.ijhydene.2022.01.229

capacities, the nanotube and torusene gravimetric capacities are larger than those of the slit-shaped pore below 5 Å and smaller above 5 Å.

To explain these different behaviours of the gravimetric and volumetric isotherms, the interaction potential energy curves of the three pores should be analyzed. Fig. 11 is a plot of the interaction potential energy curves in the interior of the three pores.

These three pore shapes have the same diameter or pore width. The curved surfaces of the nanotube and torusene interact more with the H_2 molecule than the flat surfaces of the slit-shaped pores (See Fig. 11): The interaction of H_2 inside torusenes and nanotubes is about −0.13 eV/molecule and inside the slit-shaped pore is about −0.07 eV/molecule. A deeper potential implies, in general, a larger number of stored hydrogen molecules, in the same volume of space, or in another words, a larger volumetric capacity, up to some high value of the pressure. At high pressures, the interactions between the molecules are more intense and the width of the potentials must be also considered. The potential of the slit-shaped pore is wider than the potentials of the nanotube and torusene. This implies, in general, more room to store molecules than the other two types of pores at high pressures. Hence, these differences in the potentials explain that the volumetric capacities of the torusene and nanotube are larger than those of the slit-shaped pore of the same width up to 32 MPa and smaller for pressures larger than 32 MPa (See Fig. 10).

About the gravimetric storage capacities, these capacities also depend on the mass of the adsorbent material in the same volume of space. The amount of mass of the adsorbent material is higher in the nanotube and torusene than in the slit-shaped pore and therefore, the result is that the gravimetric capacities of the slit-shaped pore is higher than those of the nanotube and torusene.

One of the important factors on the hydrogen storage capacities of nanoporous solid materials is the surface of the materials. One goal is to increase the surface of the materials that interacts with the hydrogen molecules. To reach that goal, it is relevant to find an optimal geometry of the pores. The geometry is optimal when the potential wells inside the pores are deep and wide. A specific and approximate target is potential wells of −0.3 eV/molecule [68]. The interaction of one molecule with a graphene-like surface is approximately −0.03 or −0.04 eV/molecule. The potential wells inside narrow nanotubes and torusenes are about −0.13 eV/molecule deep. Hence, it can be estimated that the interaction of narrow torusenes and nanotubes with H_2 is equivalent to the interaction of several graphene-like surfaces with H_2 at the same time.

The histograms of the molecules inside the three types of pores are plotted in Fig. 12. The histograms of the nanotube and the torusene are very similar. In the three types of pores, there is only one H_2 layer and is located at the center of the pore. The width of the layer is about 1.4 Å for the nanotube and torusene and about 1.6 Å for the slit-shaped pore. The layers of stored hydrogen of the nanotube and torusene are higher than the layer of the slit-shaped pore. The width and the height of the layers are correlated with the interaction potential: The interaction potential of the slit-shaped pore is a bit wider and less deep than the interaction potentials of the other two types of pores (See Fig. 11) and this implies that the layer of stored hydrogen is a bit wider and has a lower height, respectively, in the case of the slit-shaped pore. The histograms of the nanotube and torusene have two peaks or maxima and there is a local minimum between them, located at the center of the pore. The histogram of the slit-shaped pore has only one peak and is also located at the center of the pore. The histogram of the slit-shaped at 6.78 Å, with one hydrogen layer and located in the center of the pore, is similar to the histogram or density profile obtained by Karki and Chakraborty [45] and Rzepka et al. [56] at room temperatures for a slit-shaped pore of 7 Å.

Hydrogen storage capacities of wide slit-shaped pores, nanotubes, torusenes and spherical pores of the same size as a function of the pressure

The storage capacities of the pores depend on their size or diameter. In the above section, the capacities of narrow pores were studied. Hence, it makes sense to study also the

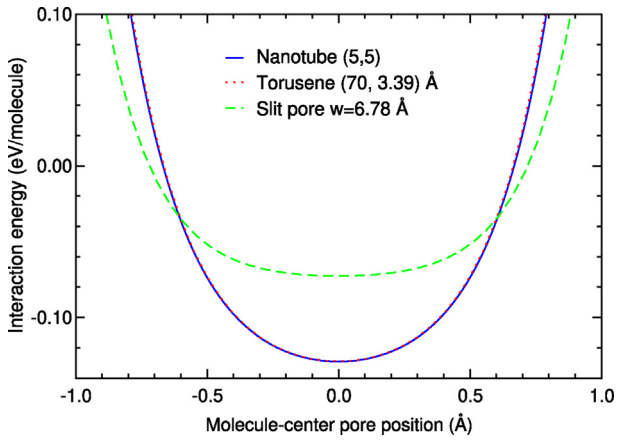

Fig. 11 – Interaction potential energy inside three pore shapes with a pore width or diameter of 6.78 Å.

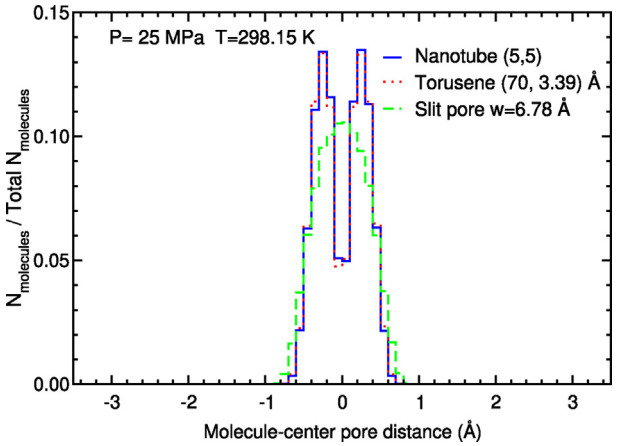

Fig. 12 – Normalized histogram of the molecules inside three pore shapes with a pore width or diameter of 6.78 Å, at 25 MPa and 298.15 K.

Please cite this article as: Caviedes D, Cabria I, Grand Canonical Monte Carlo simulations of the hydrogen storage capacities of slit-shaped pores, nanotubes and torusenes, International Journal of Hydrogen Energy, https://doi.org/10.1016/j.ijhydene.2022.01.229

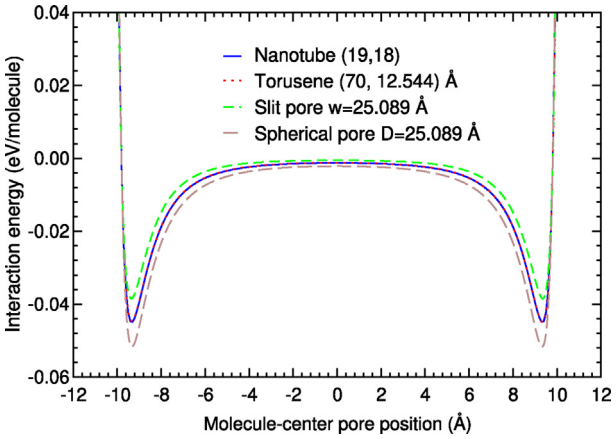

Fig. 13 – Interaction potential energy inside four pore shapes with a pore width or diameter of 25.089 Å.

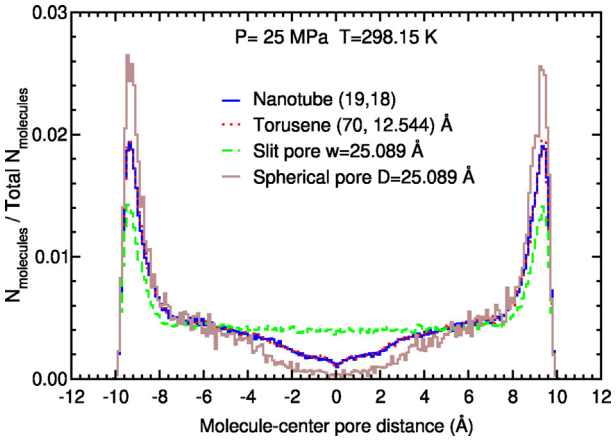

Fig. 14 – Histogram of the molecules inside four pore shapes with a pore width or diameter of 25.089 Å, at 25 MPa and 298.15 K.

capacities of wide pores. The results of the GCMC simulations of four types of pore shapes (slit-shaped pore, nanotube, torusene and spherical pore), with the same diameter, 25.089 Å, are plotted and compared in Figs. 13–15. The reason to choose a diameter of 25.089 Å for the four pores was that, as it was explained in a former subsection, the nanotube (19,18) has a diameter of 25.089 Å and is the nanotube with the closest diameter to 25 Å.

The potentials of the four pore shapes are plotted in Fig. 13. The potential of the spherical pore is more intense than the other three potentials. The different curvature of the pores has a larger impact on the potentials of narrow pores than in the potentials of wide pores. The overlap of the potentials due to the opposite surfaces is stronger on narrow pores than on wide pores and this explains that the curvature has a larger impact on the storage capacities of narrow pores.

The histograms of the molecules inside the four types of pores (See Fig. 14) show the presence of two high or dense H_2 layers located close to the borders or surfaces of the pore (about 3 Å from the border or surface), and many less dense H_2 layers inside the pore, between the two mentioned main H_2 layers. Similar histograms or density profiles were obtained in previous GCMC simulations at room temperature for slit-shaped pores of 10 and 15 Å [45] and 14 and 20 Å [56]: Two dense hydrogen layers located at about 3 Å from the graphene sheets of slit-shaped pores. The location of the maxima of the four histograms coincide with the minima of the interaction potentials of the four types of pores, as can be noticed by comparing Figs. 13 and 14. The histograms of the nanotube and torusene with a pore diameter of 25.089 Å are very similar.

The storage capacities obtained in the GCMC simulations of the four wide pores at plotted and compared in Fig. 15. Analyzing the potentials of the four wide pores of this section, one could expect similar capacities for the four pores. In fact, the volumetric capacities are very similar. The volumetric capacities of the spherical pore are slightly smaller than the volumetric capacities of the other three types of pores. However, the gravimetric capacities obtained in the GCMC simulations are different.

The slit-shaped pores have larger gravimetric capacities than the other three pores at any pressure, at room temperature. The gravimetric capacities of slit-shaped pores are about two times larger than those of nanotubes and torusenes. Nanotube and torusene have very similar gravimetric capacities and the spherical pores have the smallest gravimetric capacities at any pressure.

These differences between the gravimetric capacities of the three shapes of pores can be explained taking into account three variables of these pores: The volumetric capacities, the

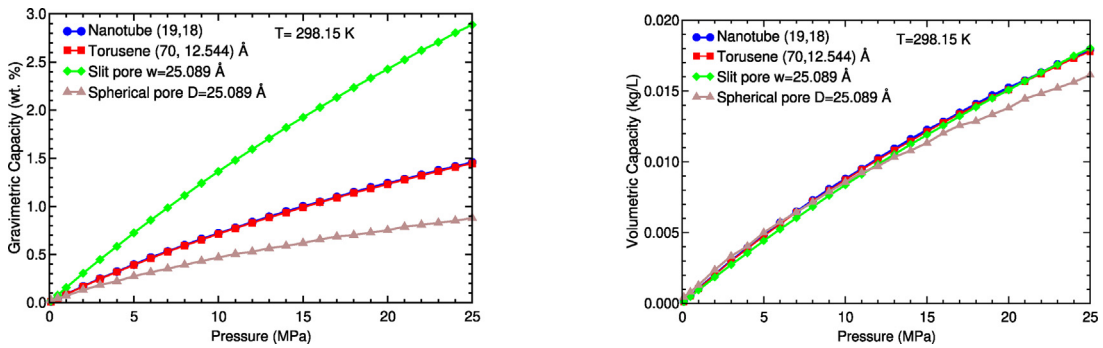

Fig. 15 – Total gravimetric and volumetric storage capacities of four pore shapes as a function of the pressure, at 298.15 K and for a width or diameter of 25.089 Å.

Please cite this article as: Caviedes D, Cabria I, Grand Canonical Monte Carlo simulations of the hydrogen storage capacities of slit-shaped pores, nanotubes and torusenes, International Journal of Hydrogen Energy, https://doi.org/10.1016/j.ijhydene.2022.01.229

surface mass densities and the volume/surface ratio of the simulation cells.

The gravimetric capacity obtained in the present GCMC simulations is defined by:

$$g_c = 100\frac{mass_{Hstored}}{mass_{Hstored} + mass_{adsorbentmaterial}}, \quad (3)$$

where $mass_{Hstored}$ is the mass of stored hydrogen and $mass_{adsorbentmaterial}$ is the mass of the adsorbent material. The gravimetric capacity can be approximated by:

$$g_c \approx 100\frac{mass_{Hstored}}{mass_{adsorbentmaterial}}, \quad (4)$$

because $mass_{Hstored}$ is much smaller than $mass_{adsorbentmaterial}$. The mass of stored hydrogen is equal to $V\rho_{H_2}$, where V is the volume of the pore and ρ_{H_2} is the volumetric capacity or density of stored hydrogen. The mass of the adsorbent material is equal to $S\sigma_{adsorbent}$, where S is the surface of the pore and $\sigma_{adsorbent}$ is the surface mass density of the pore (or the surface mass density of the adsorbent material). Hence, the gravimetric capacity is approximately equal to:

$$g_c \approx 100f\frac{\rho_{H_2}}{\sigma_{adsorbent}}, \quad (5)$$

where $f = V/S$ is the volume/surface ratio. To compare the gravimetric capacities of the pores, the ratio of the gravimetric capacities is necessary. The ratio $r_{gc}(pore)$ is defined as:

$$r_{gc}(pore) = g_c(pore)/g_c(slit), \quad (6)$$

where the gravimetric capacities are those of a pore and of a slit-shaped pore of the same width or diameter and at the same pressure and temperature.

According to the GCMC simulations, the density of stored hydrogen, or volumetric capacity, ρ_{H_2}, is approximately the same for the four types of pores with the same diameter and at the same pressure and temperature (See Fig. 15). The four pores have also approximately the same value for $\sigma_{adsorbent}$. Therefore, from Eq. (5), the following approximation is obtained:

$$r_{gc}(pore) = g_c(pore)/g_c(slit) \approx f(pore)/f(slit);, \quad (7)$$

where f is the volume/surface ratio of the corresponding pore shape.

The ratio $f(pore)/f(slit)$ of the simulation cells and the ratio $r_{gc}(pore)$ obtained in the GCMC simulations of the four pores at 25 MPa and 298.15 K are shown in Table 3. The ratio $f(pore)/f(slit)$ is the same for any pressure and temperature, because it depends only on the geometry of the pore. It can be noticed in that table that the ratio $r_{gc}(pore)$ at 25 MPa is approximately equal to $f(pore)/f(slit)$, in agreement with the approximate equation (7).

Table 3 – Volume, surface and volume/surface ratio f equations and ratio $f(pore)/f(slit)$ of the simulation cells and ratio $r_{gc}(pore)$ obtained in the GCMC simulations of the four wide pores, D = 25.089 Å, at 25 MPa and 298.15 K.

Pore	Volume	Surface	f	$f(pore)/f(slit)$	$r_{gc}(pore)$
Slit	SD	$2S$	$D/2$	1.0000	1.0000
Nanotubes	$\pi r^2 L$	$2\pi rL$	$D/4$	0.5000	0.5049
Torusenes R = 70	$2\pi^2 r^2 R$	$4\pi^2 rR$	$D/4$	0.5000	0.5007
Spherical Pore	$4\pi r^3/3$	$4\pi r^2$	$D/6$	0.3333	0.3052

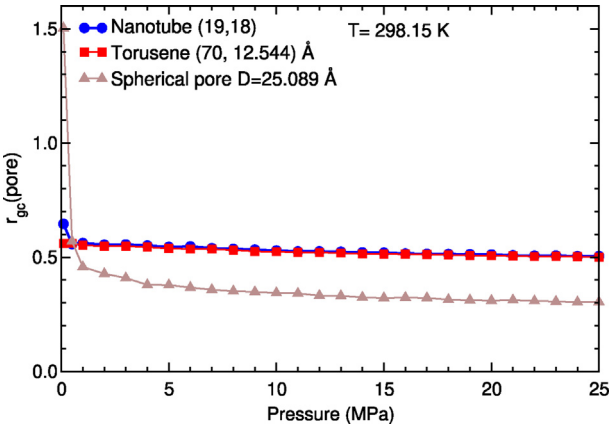

Fig. 16 – Ratio $r_{gc}(pore)$ of the nanotube, torusene and spherical pores with a width or diameter of 25.089 Å, as a function of the pressure.

The ratio $r_{gc}(pore)$ obtained in the GCMC simulations at 298.15 K as a function of the pressure for the nanotube, torusene and spherical pores is shown in Fig. 16. The ratio $r_{gc}(pore)$ of nanotube and torusene tends quickly towards the value of $f(pore)/f(slit)$ for nanotubes and torusenes, 0.5, as the pressure increases (See Table 3). The ratio $r_{gc}(pore)$ of the spherical pore tends towards 0.3000 as the pressure increases, close to the value of $f(pore)/f(slit)$, 0.3333, predicted by the approximate equation (7). There is some disagreement with the approximate equation at low pressures for the nanotube and a very strong disagreement at low pressures for the spherical pore.

The results shown on Table 3 and Fig. 16 indicate that, the relationship $r_{gc}(pore) \approx f(pore)/f(slit)$ is valid at medium and high pressures ($P \geq 5$ MPa) and for wide pores, and also indicate, as it was stated above, that the differences between the gravimetric capacities of wide pores are related to the volumetric capacities, the mass surface density and the volume/surface ratio. The relationship $r_{gc}(pore) \approx f(pore)/f(slit)$, is one of the sought structure-storage capacity relationships. The present GCMC simulations have been useful to obtain and confirm that relationship.

Conclusions and future lines

The gravimetric and volumetric storage capacities of torusenes obtained in the present GCMC simulations at 298.15 K and the interaction potential energy curves of torusenes are practically independent of the external radius R of the torusenes, for any value of the internal radius r and the pressure.

The torusenes and nanotubes with the same internal radius r have very similar interaction potential energy curves inside them and also very similar gravimetric and volumetric capacities at any pressure and 298.15 K, according to the GCMC simulations.

The gravimetric capacities of torusenes, nanotubes and slit-shaped pores at 298.15 K and 25 MPa obtained in the GCMC

Please cite this article as: Caviedes D, Cabria I, Grand Canonical Monte Carlo simulations of the hydrogen storage capacities of slit-shaped pores, nanotubes and torusenes, International Journal of Hydrogen Energy, https://doi.org/10.1016/j.ijhydene.2022.01.229

simulations have a local maximum at approximately the same pore width or diameter, 6.8 Å. The volumetric capacities of these three types of pores have the global maximum at approximately the same pore width, which is also 6.8 Å. The volumetric capacities of torusenes, nanotubes and slit-shaped pores at 298.15 K as a function of the pore width tend towards a very similar value, as the pore width increases. These results suggest that there are two features of the storage capacities of carbon pores that are independent of the pore shape: a) The optimal pore size for volumetric and gravimetric capacities and b) the volumetric capacity of wide pores.

Finally, the storage capacities of wide pores with four pore shapes, slit-shaped pores, nanotubes, torusenes and spherical pores, obtained in the GCMC simulations at 298.15 K have been compared. The comparison and analysis of the capacities of these four pore shapes indicates that there is a structure-storage capacity relationship at medium and high pressures and at 298.15 K: $r_{gc}(pore) \approx f(pore)/f(slit)$, where $g_c(pore)$ and $g_c(slit)$ are the gravimetric storage capacities of the corresponding pore shape and of the slit-shaped pore, respectively, and $f(pore)$ and $f(Slit)$ are the volume/surface ratios of the corresponding pore shape and of the slit-shaped pore, respectively.

GCMC simulations of the hydrogen storage capacities of carbon pores with another shapes and another carbon nanostructures will be carried out to confirm the conclusions obtained in this research: Schwarzites, nano-onions, nanocones, slit pores with double and triple layers, slit pores made of finite layers and double nanotubes, among other.

Declaration of competing interest

The authors declare that they have no known competing financial interests or personal relationships that could have appeared to influence the work reported in this paper.

Acknowledgments

This work was founded by MICINN research project from Spain (Grant PGC2018-093745-B-I00), Junta de Castilla y León (Grant VA124G18) and the University of Valladolid, Spain. The use of the computer facilities of Centro de Proceso de Datos - Parque Científico of the University of Valladolid is acknowledged.

Appendix. Generation of the Coordinates of the Torusenes

The coordinates of the carbon atoms of the torusenes have been generated as follows. First, the number of carbon atoms, n, on the surface of the toroid is calculated such that the surface density of carbon atoms is equal to the surface density of carbon atoms on graphene. Second, the initial coordinates on the surface of the toroid are generated according to the Fibonacci lattice algorithm [69–72].

That algorithm generates pairs of point (u, v) in a unit square, i.e., u and v are between 0 and 1 and are defined as follows:

$$\begin{aligned} u &= frac(i/\varphi) \\ v &= i/n, \end{aligned} \tag{8}$$

where $frac(x)$ is the fractional part of x, i runs between 1 and n, and φ is the golden section or golden ratio number. n is the number of points; in our case, n is the above mentioned number of carbon atoms on the surface of the torusene.

The pairs (u, v) are, then, mapped into the surface of a torusene with major radius R and minor radius r.

A differential element on the surface of a torusene is given by:

$$dS = (R + rcos\alpha)rd\alpha d\beta. \tag{9}$$

This element is equal to $dwd\beta$, where dw is given by:

$$dw = (R + rcos\alpha)rd\alpha. \tag{10}$$

Integrating this element, the variable w is obtained:

$$w = Rr\alpha + r^2 sin\alpha. \tag{11}$$

This variable w changes between 0 and $2\pi Rr$. The variables w and β are on equal foot and hence, the pair (u, v) is mapped to the pair (w, β):

$$\begin{aligned} w &= 2\pi Rru \\ \beta &= 2\pi v. \end{aligned} \tag{12}$$

The angle α is a function of w. From Eqs. (11) and (12) the following expression is obtained:

$$2\pi Rru = Rr\alpha + r^2 sin\alpha. \tag{13}$$

The angle α is obtained by solving Eq. (13). For each (u, v) pair, a pair of angles (α, β) is obtained. This pair of angles is introduced into Eq. (2) to get the initial Cartesian coordinates of each carbon atom on the torusene surface.

The last step consists on moving randomly the initial coordinates of the atoms on the toroid surface, minimizing the total energy of the interactions between the carbon atoms. The interaction energy between two carbon atoms located at points $\vec{r_i}$ and $\vec{r_j}$ is given by:

$$E_{ij} = \sum \frac{1}{|\vec{r_i} - \vec{r_j}|^2}. \tag{14}$$

The total energy of this procedure is, then:

$$E = \sum_{i=1}^{i=n} \sum_{j,j\neq i} E_{ij}. \tag{15}$$

A random move consists on changing randomly the values of the angles α and β of one carbon atom (See Eq. (2)). One iteration in the third step consists on making a random move on each carbon atom. The third step consists on applying hundreds or thousands of iterations.

This procedure allows us to obtain a set of carbon atoms distributed on the toroid surface with an approximately constant surface density of carbon atoms, if the number of iterations is large enough. On each iteration the first, second, third and fourth nearest-neighbour C–C distances are calculated. To obtain similar first, second, third and fourth distances and hence, to obtain an approximately constant surface density of carbon atoms, thousands of iterations are needed.

Please cite this article as: Caviedes D, Cabria I, Grand Canonical Monte Carlo simulations of the hydrogen storage capacities of slit-shaped pores, nanotubes and torusenes, International Journal of Hydrogen Energy, https://doi.org/10.1016/j.ijhydene.2022.01.229

The goal behind this procedure is to build torusenes with different and continuous values of the radii R and r and with an approximately constant surface density of carbon atoms, equal to the surface density of graphene. For torusenes with a major radius $R = 20$ and 70 Å, a number of 3000 iterations have been used and for torusenes with $R = 240$ Å, 1000 iterations.

REFERENCES

[1] Office of Energy Efficiency & Renewable Energy, Fuel Cell Technologies Office. Materials-based hydrogen storage. https://www.energy.gov/eere/fuelcells/materials-based-hydrogen-storage. [Accessed 12 January 2022].
[2] Office of Energy Efficiency & Renewable Energy, Fuel Cell Technologies Office. DOE technical targets for onboard hydrogen storage for light-duty vehicles. https://www.energy.gov/eere/fuelcells/doe-technical-targets-onboard-hydrogen-storage-light-duty-vehicles. [Accessed 2 January 2022].
[3] Broom DP, Webb CJ, Fanourgakis GS, Froudakis GE, Trikalitis PN, Hirscher M. Concepts for improving hydrogen storage in nanoporous materials. Int J Hydrogen Energy 2019;44:7768–79.
[4] Toyota. https://www.toyota.com/content/ebrochure/2018/mirai_FuelCellTech.pdf. [Accessed 3 December 2021].
[5] Nijkamp MG, Raaymakers JEMJ, van Dillen AJ, de Jong KP. Hydrogen storage using physisorption - materials demands. Appl Phys A 2001;72:619–23.
[6] Züttel A. Materials for hydrogen storage. Mater Today 2003;6:24–33.
[7] Kaneko K, Rodríguez-Reinoso F, editors. Nanoporous materials for gas storage. New York: Springer Singapore; 2019.
[8] Allendorf MD, Hulvey Z, Gennett T, Ahmed A, Autrey T, Camp J, et al. An assessment of strategies for the development of solid-state adsorbents for vehicular hydrogen storage. Energy Environ Sci 2018;11:2784–812.
[9] Ren J, Musyoka NM, Langmi HW, Mathe M, Liao S. Current research trends and perspectives on materials-based hydrogen storage solutions: a critical review. Int J Hydrogen Energy 2017;42:289–311.
[10] Broom DP, Webb CJ, Hurst KE, Parilla PA, Gennett T, Brown CM, et al. Outlook and challenges for hydrogen storage in nanoporous materials. Appl Phys A 2016;122:151.
[11] Blankenship TS, Balahmar N, Mokaya R. Oxygen-rich microporous carbons with exceptional hydrogen storage capacity. Nat Commun 2017;8:1545.
[12] Sethia G, Sayari A. Activated carbon with optimum pore size distribution for hydrogen storage. Carbon 2016;99:289–94.
[13] Lan J, Cao D, Wang W, Ben T, Zhu G. High-capacity hydrogen storage in porous aromatic frameworks with diamond-like structure. J Phys Chem Lett 2010;1:978–81.
[14] Diercks CS, Yaghi OM. The atom, the molecule, and the covalent organic framework. Science 2017;355:eaal1585. https://doi.org/10.1126/science.aal1585.
[15] Li ZP, Zhi YF, Feng X, Ding XS, Zou YC, Liu XM, et al. An azine-linked covalent organic framework: synthesis, characterization and efficient gas storage. Chem Eur J 2015;21:12079–84.
[16] Lu W. Strategies for hydrogen storage in porous organic polymers. In: Nanostructured materials for next-generation energy storage and conversion hydrogen production, storage, and utilization; chap. 7. Springer; 2017. p. 203–23.
[17] Yuan D, Lu W, Zhao D, Zhou HC. Highly stable porous polymer networks with exceptionally high gas-uptake capacities. Adv Mater 2011;23:3723–5.
[18] Lu W, Yuan D, Zhao D, Schilling CI, O Plietzsch TM, Bräse S, et al. Porous polymer networks: synthesis, porosity, and applications in gas storage/separation. Chem Mater 2010;22:5964–72. https://doi.org/10.1021/cm1021068.
[19] Tian T, Zeng Z, Vulpe D, Casco ME, Divitini G, Midgley PA, et al. A sol-gel monolithic metal-organic framework with enhanced methane uptake. Nat Mater 2018;17:174–9.
[20] Zou L, Zhou HC. Hydrogen storage in metal-organic frameworks. In: Nanostructured materials for next-generation energy storage and conversion - hydrogen production, storage, and utilization; chap. 5. Berlin, Heidelberg: Springer-Verlag; 2017. p. 143–70.
[21] Ramimoghadam D, Gray E, Webb J. Review of polymers of intrinsic microporosity for hydrogen storage applications. Int J Hydrogen Energy 2016;41:16944–65. https://doi.org/10.1016/j.ijhydene.2016.07.134.
[22] McKeown NB, Budd PM, Book D. Microporous polymers as potential hydrogen storage materials. Macromol Rapid Commun 2007;28:995–1002.
[23] Park MS, Lee SE, Kim MI, Lee YS. CO_2 adsorption characteristics of slit-pore shaped activated carbon prepared from cokes with high crystallinity. Carbon Lett 2015;16:45–50.
[24] Guo J, Morris JR, Ihm Y, Contescu CI, Gallego NC, Duscher G, et al. Topological defects: origin of nanopores and enhanced adsorption performance in nanoporous carbon. Small 2012;8:3283–8.
[25] Franklin RE. Crystallite growth in graphitizing and nongraphitizing carbons. Proc Roy Soc 1951;209:196–218.
[26] Cabria I, López MJ, Alonso JA. Simulation of the hydrogen storage in nanoporous carbons with different pore shapes. Int J Hydrogen Energy 2011;36:10748–59.
[27] Cabria I, López MJ, Alonso JA. Hydrogen storage in pure and Li-doped carbon nanopores: combined effects of concavity and doping. J Chem Phys 2008;128:144704.
[28] Chen L, Wang H, Xu J, Shen X, Yao L, Zhu L, et al. Controlling reversible elastic deformation of carbon nanotube rings. J Am Chem Soc 2011;133:9654–7.
[29] Zheng M, Ke C. Elastic deformation of carbon-nanotube nanorings. Small 2010;6:1647–55.
[30] Geng J, Ko YK, Youn SC, Kim YH, Kim SA, Jung DH, et al. Synthesis of SWNT rings by noncovalent hybridization of porphyrins and single-walled carbon nanotubes. J Phys Chem C 2008;112:12264–71.
[31] Yu H, Zhang Q, Luo G, Wei F. Rings of triple-walled carbon nanotube bundles. Appl Phys Lett 2006;89:223106.
[32] Colomer JF, Henrard L, Flahaut E, Tendeloo GV, Lucas AA, Lambin P. Rings of double-walled carbon nanotube bundles. Nano Lett 2003;3:685–9.
[33] Sano M, Kamino A, Okamura J, Shinkai S. Ring closure of carbon nanotubes. Science 2001;293:1299–301.
[34] Martel R, Shea HR, Avouris P. Rings of single-walled carbon nanotubes. Nature 1999;398:299.
[35] Martel R, Shea HR, Avouris P. Ring formation in single-wall carbon nanotubes. J Phys Chem B 1999;103:7551–6.
[36] Liu J, Dai HJ, Hafner JH, Colbert DT, Smalley RE, Tans SJ, et al. Fullerene 'crop circles. Nature 1997;385:780–1. https://doi.org/10.1038/385780b0.
[37] Silveira JFRV, Muniz AR. Chain- and chainmail-like nanostructures from carbon nanotube rings. Comput Mater Sci 2019;161:76–82.
[38] Cox BJ, Hill JM. New carbon molecules in the form of elbow-connected nanotori. J Phys Chem C 2007;111:10855–60.

Please cite this article as: Caviedes D, Cabria I, Grand Canonical Monte Carlo simulations of the hydrogen storage capacities of slit-shaped pores, nanotubes and torusenes, International Journal of Hydrogen Energy, https://doi.org/10.1016/j.ijhydene.2022.01.229

[39] László I, Rassat A, Fowler PW, Graovac A. Topological coordinates for toroidal structures. Chem Phys Lett 2001;342:369–74.
[40] Marušišc D, Pisanski T. Symmetries of hexagonal molecular graphs on the torus. Croat Chem Acta 2000;73:969–81.
[41] Graovac A, Plavšić D, Kaufman M, Pisanski T, Kirby EC. Application of the adjacency matrix eigenvectors method to geometry determination of toroidal carbon molecules. J Chem Phys 2000;113:1925–31.
[42] Han J. Toroidal single walled carbon nanotubes in fullerene crop circles. NASA Advanced Supercomputing; 1997. Technical Report.
[43] Kirby EC. Recent work on toroidal and other exotic fullerene structures. In: Balaban AT, editor. From chemical topology to three-dimensional geometry. New York: Plenum; 1997. p. 263–96.
[44] Kirby EC, Mallion RB, Pollak P. Toroidal polyhexes. J Chem Soc Faraday Trans 1993;89:1945–53.
[45] Karki S, Chakraborty SN. A Monte Carlo simulation study of hydrogen adsorption in slit-shaped pores. Microporous Mesoporous Mater 2021;317:110970. https://doi.org/10.1016/j.micromeso.2021.110970.
[46] Wu X, Wang Y, Cai Z, Zhao D, Cai W. Revealing enhancement mechanism of volumetric hydrogen storage capacity of nano-porous frameworks by molecular simulation. Chem Eng Sci 2020;226:115837. https://doi.org/10.1016/j.ces.2020.115837.
[47] Krasnov PO, Shkaberina GS, Kuzubov AA, Kovaleva EA. Molecular hydrogen sorption capacity of D-schwarzites. Appl Surf Sci 2017;416:766–71.
[48] Sriling P, Wongkoblap A, Tangsathitkulchai C. Computer simulation study for methane and hydrogen adsorption on activated carbon based catalyst. Adsorption 2016;22:707–15.
[49] Ozturk Z, Baykasoglu C, Kirca M. Sandwiched graphene-fullerene composite: a novel 3-D nanostructured material for hydrogen storage. Int J Hydrogen Energy 2016;41:6403–11. https://doi.org/10.1016/j.ijhydene.2016.03.042.
[50] Bartolomei M, Carmona-Novillo E, Giorgi G. First principles investigation of hydrogen physical adsorption on graphynes' layers. Carbon 2015;95:1076–81.
[51] Robledo CB, Rojas MI, Cámara O, Leiva EPM. First-principles studies concerning optimization of hydrogen storage in nanoporous reduced graphite oxide. Int J Hydrogen Energy 2014;39:4396–403.
[52] Kumar KV, Salih A, Lu L, Müller EA, Rodríguez-Reinoso F. Molecular simulation of hydrogen physisorption and chemisorption in nanoporous carbon structures. Adsorpt Sci Technol 2011;29:799–817.
[53] García Blanco AA, de Oliveira JCA, López R, Moreno-Piraján JC, Giraldo L, Zgrablich G, et al. A study of the pore size distribution for activated carbon monoliths and their relationship with the storage of methane and hydrogen. Colloids Surf A Physicochem Eng Asp 2010;357:74–83. https://doi.org/10.1016/j.colsurfa.2010.01.006.
[54] Cracknell RF. Molecular simulation of hydrogen adsorption in graphitic nanofibres. Phys Chem Chem Phys 2001;3:2091–7. https://doi.org/10.1039/B100144M.
[55] Wang Q, Johnson JK. Molecular simulation of hydrogen adsorption in single-walled carbon nanotubes and idealized carbon slit pores. J Chem Phys 1999;110:577–86.
[56] Rzepka M, Lamp P, de la Casa-Lillo MA. Physisorption of hydrogen on microporous carbon nanotubes. J Phys Chem B 1998;102:10894–8.
[57] Frenkel D, Smit B. Understanding molecular simulation. From algorithms to applications. New York, NY: Academic Press; 2002.
[58] Lennard-Jones JE. On the determination of molecular fields. Proc Roy Soc 1924;106:463–77. https://doi.org/10.1098/rspa.1924.0082.
[59] Steele WA. The physical interaction of gases with crystalline solids: I. Gas-solid energies and properties of isolated adsorbed atoms. Surf Sci 1973;36:317–52.
[60] Tjatjopoulos GJ, Feke DL, Mann Jr JA. Molecule-micropore interaction potentials. J Phys Chem 1988;92:4006. https://doi.org/10.1021/j100324a063.
[61] Siderius DW, Gelb LD. Extension of the steele 10-4-3 potential for adsorption calculations in cylindrical, spherical, and other pore geometries. J Chem Phys 2011;135:084703.
[62] Soave G. Equilibrium constants from a modified Redlich-Kwong equation of state. Chem Eng Sci 1972;27:1197–203.
[63] Zhou L, Zhou Y. Determination of compressibility factor and fugacity coefficient of hydrogen in studies of adsorptive storage. Int J Hydrogen Energy 2001;26:597–601.
[64] Moore SG, Wheeler DR. Chemical potential perturbation: a method to predict chemical potentials in periodic molecular simulations. J Chem Phys 2011;134:114514.
[65] Metropolis N. The beginning of the Monte Carlo method. Los Alamos Sci 1987;15:125–30.
[66] Papadimitriou NI, Tsimpanogiannis IN, Stubos AK. Monte Carlo study of sI hydrogen hydrates. Mol Simulat 2010;36:736–44. https://doi.org/10.1080/08927021003752796.
[67] Allen MP, Tildesley DJ. Computer simulation of liquids. Oxford: Oxford University Press; 1987.
[68] Li J, Furuta T, Goto H, Ohashi T, Fujiwara Y, Yip S. Theoretical evaluation of hydrogen storage capacity in pure carbon nanostructures. J Chem Phys 2003;119:2376–85.
[69] Dixon R. Green spirals. In: Hargittai I, Pickover CA, editors. Spiral symmetry. Singapore: World Scientific; 1992. p. 353–68.
[70] Dixon R. Spiral phyllotaxis. Comput Math Appl 1989;17:535–8.
[71] Dixon R. Mathographics. Oxford: Basil Blackwell; 1987.
[72] Ridley JN. Packing efficiency in sunflower heads. Math Biosci 1982;58:129–39.

Please cite this article as: Caviedes D, Cabria I, Grand Canonical Monte Carlo simulations of the hydrogen storage capacities of slit-shaped pores, nanotubes and torusenes, International Journal of Hydrogen Energy, https://doi.org/10.1016/j.ijhydene.2022.01.229